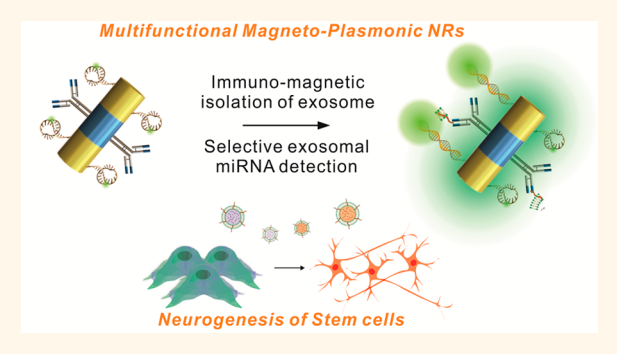


# Nondestructive Characterization of Stem Cell Neurogenesis by a Magneto-Plasmonic Nanomaterial-Based Exosomal miRNA Detection

Jin-Ho Lee,  $^{\dagger,\ddagger,\parallel_{\textcircled{\tiny{0}}}}$  Jin-Ha Choi,  $^{\dagger,\ddagger,\parallel_{\textcircled{\tiny{0}}}}$  Sy-Tsong Dean Chueng,  $^{\dagger_{\textcircled{\tiny{0}}}}$  Thanapat Pongkulapa,  $^{\dagger_{\textcircled{\tiny{0}}}}$  Letao Yang,  $^{\dagger_{\textcircled{\tiny{0}}}}$  Hyeon-Yeol Cho,  $^{\dagger,\ddagger_{\textcircled{\tiny{0}}}}$  Jeong-Woo Choi,  $^{*,\ddagger_{\textcircled{\tiny{0}}}}$  and Ki-Bum Lee\*,  $^{\dagger,\$_{\textcircled{\tiny{0}}}}$ 

Supporting Information

ABSTRACT: The full realization of stem cell-based treatments for neurodegenerative diseases requires precise control and characterization of stem cell fate. Herein, we report a multifunctional magneto-plasmonic nanorod (NR)-based detection platform to address the limitations associated with the current destructive characterization methods of stem cell neurogenesis. Exosomes and their inner contents have been discovered to play critical roles in cell—cell interactions and intrinsic cellular regulations and have received wide attention as next-generation biomarkers. Moreover, exosomal microRNAs (miRNA) also offer an essential avenue for nondestructive molecular analyses of cell cytoplasm components. To this end, our developed non-



destructive, selective, and sensitive detection platform has (i) an immunomagnetic active component for exosome isolation and (ii) a plasmonic/metal-enhanced fluorescence component for sensitive exosomal miRNA detection to characterize stem cell differentiation. In a proof-of-concept demonstration, our multifunctional magneto-plasmonic NR successfully detected the expression level of miRNA-124 and characterized neurogenesis of human-induced pluripotent stem cell-derived neural stem cells in a nondestructive and efficient manner. Furthermore, we demonstrated the versatility and feasibility of our multifunctional magneto-plasmonic NRs by characterizing a heterogeneous population of neural cells in an *ex vivo* rodent model. Collectively, we believe our multifunctional magneto-plasmonic NR-based exosomal miRNA detection platform has a great potential to investigate the function of cell—cell interactions and intrinsic cellular regulators for controlling stem cell differentiation.

KEYWORDS: magneto-plasmonic nanorods, exosomal miRNAs, stem cells, neuronal differentiation, nondestructive characterization

Ithough stem cells hold great potential for the treatment of neurodegenerative diseases and central nervous system (CNS) injuries, <sup>1-4</sup> precise control and characterization of stem cell fate are critical issues that need to be addressed before their therapeutic potential can be fully realized. <sup>5-8</sup> The current characterization methods for stem cell biomarkers are intrinsically destructive to cellular activities and functions, which then limits further analyses and biomedical applications. <sup>9,10</sup> Therefore, the discovery of new biomarker molecules and the corresponding detection methods, which can be utilized without compromising cellular vitality, would be essential for the effective analysis of stem cell differentiation into specific cell lineages. Recent studies show that cell—cell interactions and intrinsic cellular regulators are critical for

controlling stem cell neurogenesis through noncoding RNAs [e.g., microRNAs (miRNAs)]. The example, miRNAs in stem cell-derived exosomes are one of the key regulators during stem cell neurogenesis. Interestingly, exosomes, actively secreted by mammalian cells including stem cells, have emerged as an interesting cellular component for intercellular communication. These membrane-bound phospholipid nanovesicles (approximately 50–100 nm in diameter) are physically stable and composed of critical signaling molecules (including

Received: March 9, 2019 Accepted: July 30, 2019 Published: July 30, 2019



<sup>&</sup>lt;sup>†</sup>Department of Chemistry and Chemical Biology, Rutgers University, Piscataway, New Jersey 08854, United States

<sup>&</sup>lt;sup>‡</sup>Department of Chemical and Biomolecular Engineering, Sogang University, Seoul 04107, Republic of Korea

<sup>&</sup>lt;sup>§</sup>Department of Life and Nanopharmaceutical Science, College of Pharmacy, Kyung Hee University, Seoul 02447, Republic of Korea

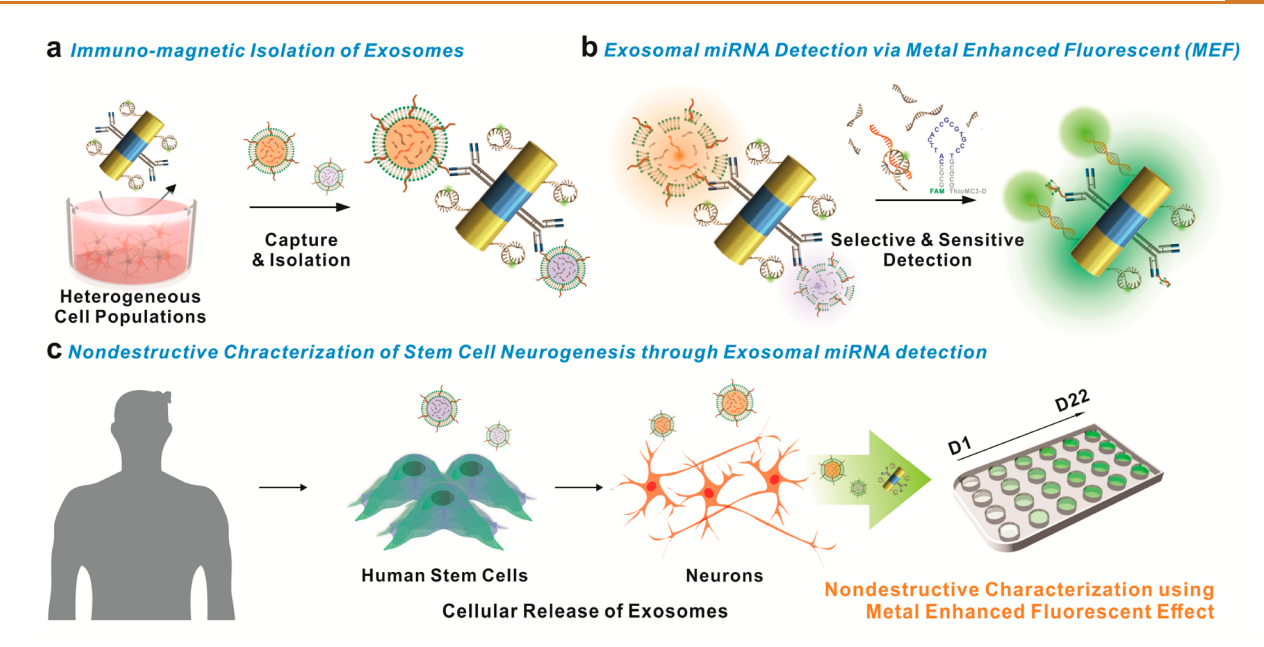


Figure 1. Schematic diagram illustrating the nondestructive, selective, and sensitive characterization of stem cell differentiation through exosomal miRNA detection. Multifunctional magneto-plasmonic nanorods are utilized to (a) extract and concentrate exosomes immunomagnetically, (b) analyze exosomal miRNA sensitively *via* metal-enhanced fluorescence effect, and (c) monitor stem cell differentiation nondestructively.

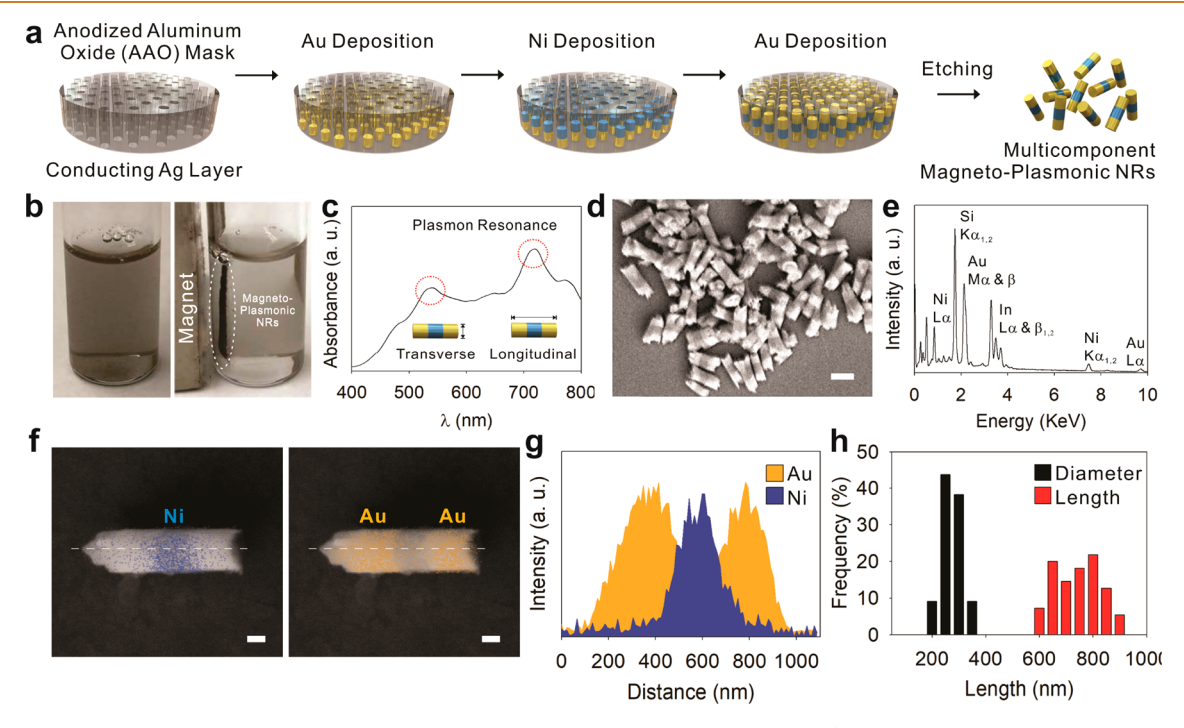


Figure 2. Generation and characterization of multicomponent magneto-plasmonic nanorods. (a) Schematic illustration of sequential steps to generate multicomponent magneto-plasmonic NRs using an electrochemical deposition method on an anodized aluminum oxide template. (b) Optical image of magnetophoretic separation property of multicomponent magneto-plasmonic NRs. (c) Corresponding UV-vis-NIR absorption spectrum of multicomponent magneto-plasmonic NRs. (d) Representative SEM image of multicomponent magneto-plasmonic NRs (scale bar: 200 nm). (e) Energy-dispersive X-ray spectroscopy spectrum (EDS) of as-prepared multicomponent magneto-plasmonic NRs. (f) Representative SEM images of single multicomponent magneto-plasmonic NR and corresponding EDS element mappings (scale bar: 100 nm). (g) EDS elemental line profiles of multicomponent magneto-plasmonic NRs. (h) Size distributions (diameter and length) of as-synthesized multicomponent magneto-plasmonic NRs.

proteins, RNAs, and DNAs) to facilitate cell—cell communication. <sup>17</sup> Notably, recent evidence suggests the importance of the small noncoding RNAs (miRNAs) (approximately 76% of total oligonucleotides inside of exosomes) as post-transcriptional

gene regulators, which are involved in the determination of cell fates.  $^{18-20}$  For example, researchers have demonstrated that exosomal miRNA secreted from donor cells could target acceptor cells and directly modulate gene expression.  $^{21-24}$ 

Hence, the accurate and simple analysis of exosomal molecules (especially miRNAs) from each cell stage would be a key prerequisite for a better understanding of cell—cell communication and the function of stem cell microenvironments on stem cell behaviors. However, current exosome analysis procedures require large sample volumes and specialized tools (such as an ultrahigh centrifuge with 100000g and a specific filtration membrane) to compensate for weak signals and poor isolation efficiency. <sup>17,25–27</sup> To this end, an innovative isolation and detection approach for exosomal miRNA in a nondestructive, selective, and sensitive manner is of great value for stem cell-based therapies.

Addressing the challenges above, we developed a method to characterize the stem cell differentiation process in a nondestructive manner using multifunctional magneto-plasmonic nanorod (NR)-based detection of exosomal miRNA in both a selective and sensitive manner [Figure 1]. For this purpose, homogeneous magneto-plasmonic NRs were synthesized by utilizing an anodized aluminum oxide (AAO) template method. We carefully designed a magnetic (nickel, Ni) component in the middle of the magneto-plasmonic NRs to selectively capture and isolate targeted exosomes through magnetic immunoprecipitation [Figure 1a], while the plasmonic (gold, Au) components at both ends of the magneto-plasmonic NRs selectively and sensitively recognize targeted exosomal miRNA using a molecular beacon (MB, a fluorophore-labeled hairpin singlestranded synthetic DNA) [Figure 1b]. During the stem cell differentiation process, exosomes were immunomagnetically isolated from biological samples, allowing a significant increase in the concentration of exosomal miRNAs. Sequentially, at the surface of the multifunctional magneto-plasmonic NRs, the captured exosomes were lysed, and the exosomal miRNA was released and then hybridized by the MB on the plasmonic Au component. We hypothesized the fluorescence signal from the miRNA-MB complex could be amplified to increase signal-tonoise ratio through metal-enhanced fluorescence (MEF) effects at the plasmonic (gold, Au) component region of magnetoplasmonic NRs [Figure 1b]. Furthermore, taking advantage of the physical and optical property of magneto-plasmonic NR components, we successfully characterized stem cell neurogenesis in a nondestructive manner [Figure 1c]. In our proof-ofconcept demonstration, we characterized neuronal differentiation of human induced pluripotent stem cell-derived neural stem cells (hiPSC-NSCs) using our multifunctional magnetoplasmonic NR method to detect exosomal miRNA-124 (miR-124) signal as a neuronal biomarker.

#### **RESULTS AND DISCUSSION**

**Generation and Characterization of Multicomponent Magneto-Plasmonic Nanorods.** To develop the magneto-plasmonic NR-based efficient exosome isolation and exosomal miRNA detection method, we synthesized the homogeneous multicomponent magneto-plasmonic NRs through potentio-static electrochemical deposition utilizing AAO (pore size 0.2  $\mu$ m) as a template [Figure 2a]. The diameter and the length of the multicomponent magneto-plasmonic NRs could be independently tuned by varying the pore size of AAO templates and the applied total electrical charge, respectively [Figure S1]. Specifically, adjusting the diameter and the length of the multicomponent magneto-plasmonic NRs enabled us to tune the aspect ratio as well as the property of the localized surface plasmon resonance (LSPR). In our multicomponent magneto-plasmonic NR system, we utilized the Au–Ni–Au configuration

to protect the Ni component during the etching process.<sup>28</sup> The ferromagnetic Ni component allowed the magnetic isolation of our multicomponent magneto-plasmonic NR from solution [Figure 2b], and the LSPR-active Au component (at 540 and 720 nm) allowed fluorescence signal amplification [Figures 2c and S2]. As demonstrated, the multicomponent magnetoplasmonic NRs are a hybrid nanomaterial having orthogonal magnetic and optical properties. The distinct separation of the magnetic and plasmonic components is crucial for the orthogonal conjugation chemistry into our synthesized NRs for efficient exosome capture and selective exosomal miRNA detection. To this end, we verified the structure and distinct regions of our multicomponent magneto-plasmonic NRs through field emission scanning electron microscopy (FE-SEM) [Figure 2d]. Through energy dispersive X-ray (EDX) analysis, we proved the multicomponent magneto-plasmonic NRs to have a bimetallic multicomponent structure showing definite segregation of the Au and Ni elements [Figure 2e, f, and g]. In detail, we observed distinct X-ray emission peaks of M $\alpha$ and  $\beta$  of Au at around 2.1 keV, L $\alpha$  of Au at around 9.7 keV, L $\alpha$  of Ni at around 0.8 keV, and  $K\alpha_{1,2}$  of Ni at around 7.5 keV, which clearly demonstrated the presence of both Au and Ni components on our multicomponent magneto-plasmonic NRs. The presence of  $K\alpha_{1,2}$  of Si (silicon) at around 1.7 keV and L $\alpha$ ,  $\beta_{1,2}$ , and  $\gamma_1$  of In (indium) at around 3.3, 3.5, 3.7, and 3.9 keV was due to the sample holder (indium tin oxide-coated glass substrate) for FE-SEM imaging. We logically designed our magneto-plasmonic NRs to be larger than exosomes (30-100 nm) for extracting exosomes and concentrating them. For this purpose, the ferromagnetic Ni component was designed to be 250 nm in length and diameter. From our SEM analysis, the multicomponent magneto-plasmonic NRs had a homogeneous size distribution and were found to be 267.35  $\pm$  23.78 nm in diameter and  $745.31 \pm 89.09$  nm in length, with an aspect (ratio of length/width) ratio of 3 [Figure 2h].

Surface Functionalization of Multicomponent Magneto-Plasmonic Nanorods for miRNA Detection. The selective and sensitive detection of stem cell neurogenesis markers in a nondestructive manner is crucial for characterizing cell identities before effective clinical applications. For the nondestructive characterization of neural differentiation, on the two ends of the multifunctional magneto-plasmonic NR, we attached an miR-124 [miRNA-124]-specific MB (molecular beacon) on the surface of the plasmonic Au blocks [Table S1]. We chose miR-124 as a specific biomarker for stem cell neurogenesis due to its low expression levels in NSCs and high expression level in differentiated neurons.<sup>29</sup> For the sensitive detection of neurogenesis, we investigated the distinct LSPR property of gold nanostructures, which can both quench and enhance the fluorescence signal from the fluorophore attached. Accordingly, we designed the MB (length of complementary strands approximately 5 to 15 nm) to control the leading phenomena between quenching and enhancement of fluorescence signal.<sup>30,31</sup> Moreover, 5(6)-carboxyfluorescein (FAM) was selected as the fluorophore of our MB, as its emission band (520 nm) matches up with the transverse plasmon absorption of the magneto-plasmonic NRs (540 nm) to generate MEF effects [Figure S2]. 32,33 To maximize the MEF effect and provide a theoretical explanation, we further performed finite-difference time-domain (FDTD) simulation on the electromagnetic (EM) field surrounding the multicomponent magneto-plasmonic NRs to investigate the fluorescence signal amplification of FAM [Figure 3]. Based on the parameters derived from physical

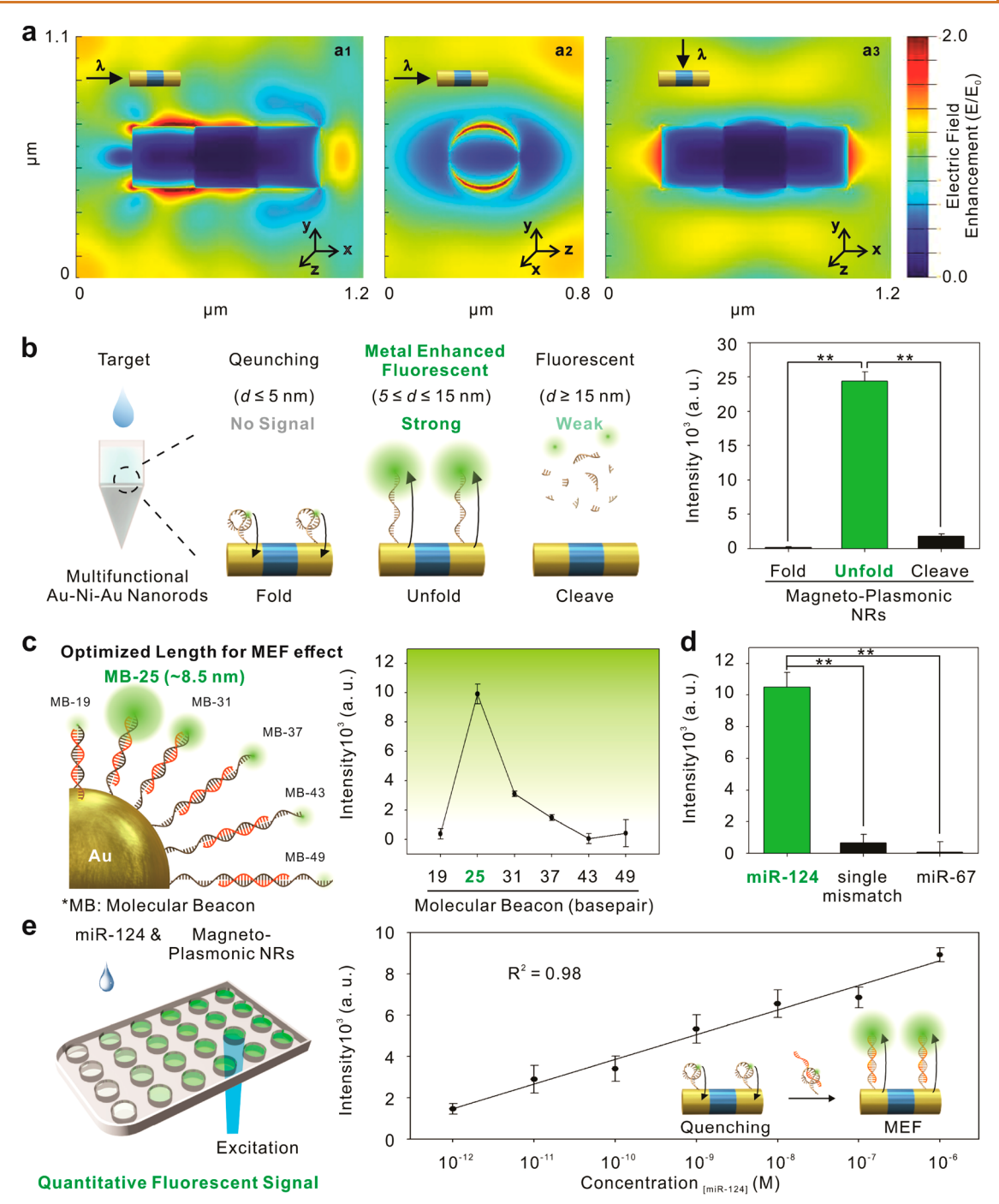


Figure 3. Surface functionalization of multicomponent magneto-plasmonic nanorods for miRNA detection. (a) Side  $(a_2)$  and top view  $(a_1)$ , and  $a_3$  of EM field intensity  $(E-E_0)$  of multicomponent magneto-plasmonic NRs under three-dimensional finite-difference time-domain simulation using 490 nm wavelength light. (b) Schematic illustration of fluorescence intensities from quenched, metal-enhanced fluorescence, and free fluorescence with respect to the folded, unfolded, and cleaved MB from the Au surface of magneto-plasmonic NRs. (c) Schematic illustration and calculated fluorescence signal intensities based on different lengths (bp) of molecular beacons. (d) Fluorescence signal value obtained from the positive complementary miR-124 DNA sequence, single mismatched synthetic DNA sequence, and mature miRNA67 DNA sequence (negative target) using a solution assay. (e) Linear correlations between concentrations (range from 1 pM to 1  $\mu$ M) of miRNA-124 and observed fluorescence signals. (The error bars represent mean  $\pm$  SD; n=3, \*\*p<0.01 by one-way ANOVA with Tukey's post hoc test.)

measurements obtained through SEM analysis, we defined the structures of the multicomponent NRs in the FDTD simulation to ensure the simulation results precisely represented the experimental conditions [Figure 2h]. The local electric field enhancement  $[(|E|/|E_0|)]$  was defined as the ratio between the near-field (|E|) intensity and the incident field ( $|E_0|$ ) intensity, which determined the extent of excitation enhancement due to

the process of MEF. The calculated EM field enhancement distribution images indicated that when multicomponent magnetic-gold NRs were exposed to incident light in either direction, longitudinal [Figure  $3a_1$  and  $a_2$ ] or transverse [Figure  $3a_3$ ], the local electric field enhancement significantly increased around the Au components.

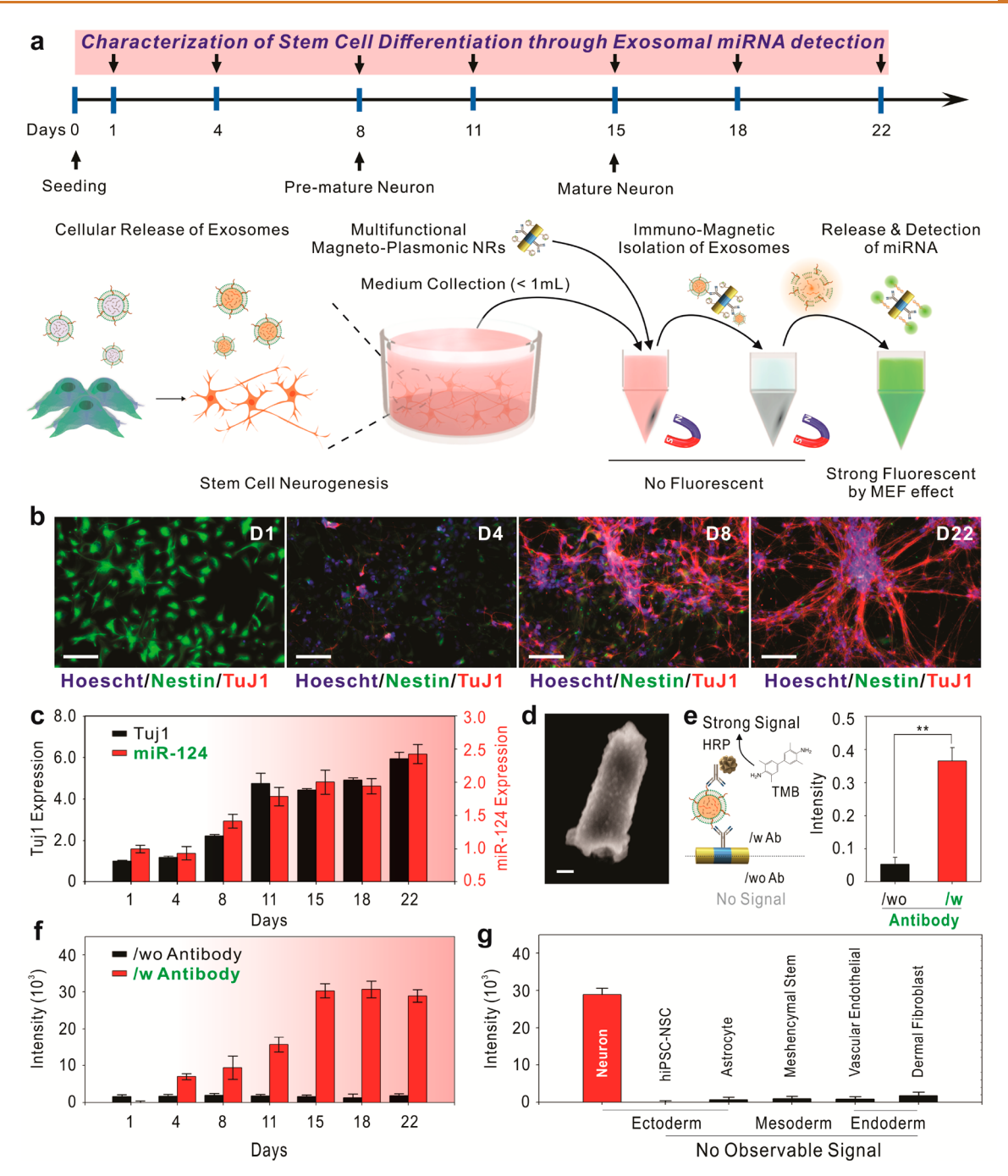


Figure 4. Nondestructive, selective, and sensitive characterization of neurogenesis of hiPSC-NSCs through immunomagnetically concentrated exosomal miRNA detection. (a) Schematic illustration of nondestructive, selective, and sensitive characterization of stem cell differentiation through immunomagnetically concentrated exosomes using multifunctional magneto-plasmonic NRs. (b) Representative immunocytochemistry images of hiPSC-NSC differentiation into neurons. Nucleus (Hoechst, blue), Nestin (Alexa Fluor 488, green), and TuJ1 (Alexa Fluor 647, red) (scale bar =  $100~\mu m$ ). (c) PCR analyses of cell lysate for a well-known neuronal marker, TuJ1, and miRNA-124 expression during the neuronal differentiation period (range from D1 to D22). (d) Representative scanning electron microscope (SEM) images of captured exosomes on the surface of multifunctional magneto-plasmonic NRs (scale bar =  $100~\mu m$ ). (e) Absorbance intensities obtained from HRP-TMB reaction (630 nm) in the absence and presence of anti-CD63 antibody on the surface of magneto-plasmonic NRs. (f) Fluorescence signals from time-dependent monitoring (range from D1 to D22) of hiPSC-NSC during neuronal differentiation. A total of  $3.0 \times 10^6$  cells were seeded on a 9.5 cm² surface area and treated with fresh hiPSC-NSC media without growth factors. (g) Fluorescence signals for other cell types from each lineage (ectoderm, neuron, hiPSC-NSC, and astrocyte; mesoderm, mesenchymal stem cell; endoderm, vascular endothelial, and dermal fibroblast). (The error bars represent mean  $\pm$  SD; n = 3, \*\*p < 0.01 by one-way ANOVA with Tukey's post hoc test.)

To verify the ability of our MB-functionalized magnetoplasmonic NRs to both quench and enhance fluorescence signal during the inactive and active states, we quantified the fluorescence signal readings from three different conditions (folded MB, unfolded MB, and cleaved MB) [Figure 3b]. By varying the temperatures, we obtained no observable fluorescence signal from the folded MB on the magneto-plasmonic NR sample due to fluorescence quenching at room

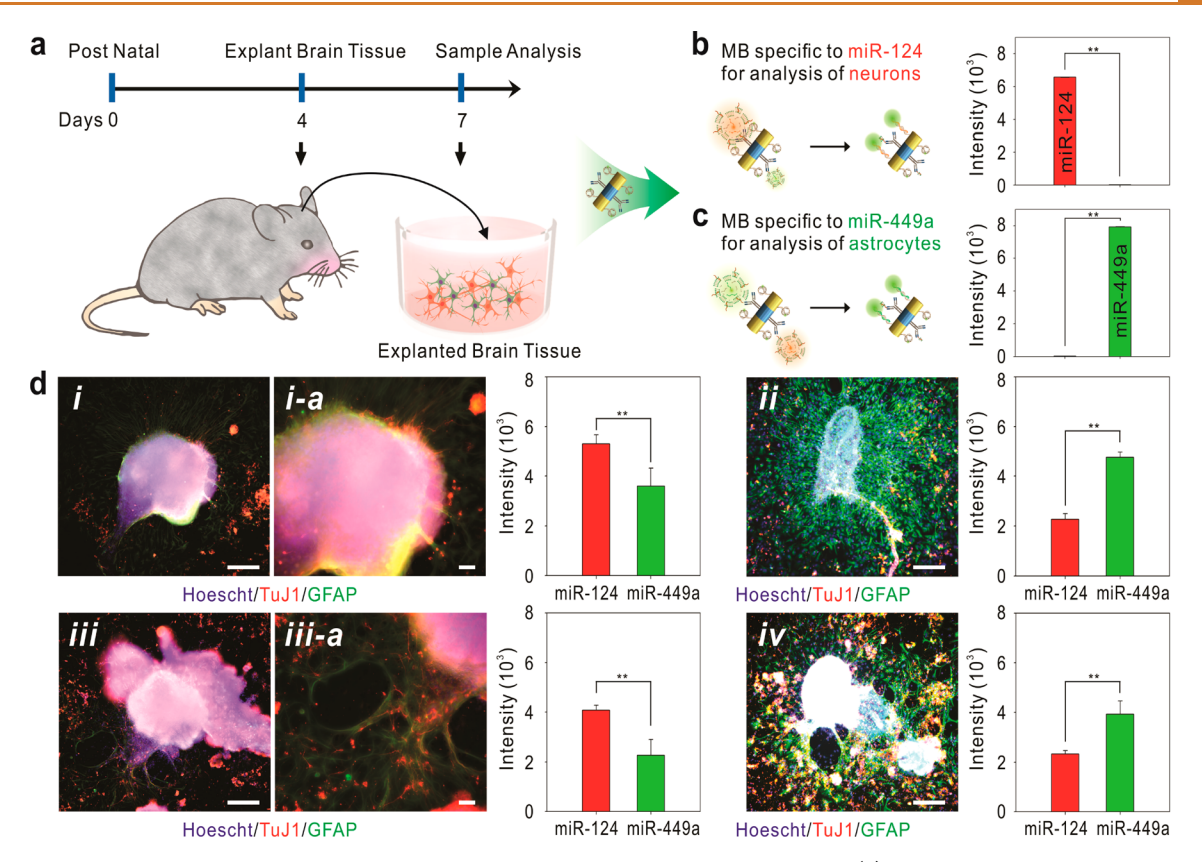


Figure 5. Nondestructive characterization of neural cell distribution in the explanted brain tissues. (a) Schematic illustration of nondestructive, selective, and sensitive characterization of dissected brain tissue explants using multifunctional magneto-plasmonic NRs. (b, c) Relative fluorescence signal values from (b) neurons and (c) astrocytes. (d) Representative immunocytochemistry staining images of brain tissue explants and relative fluorescence signals obtained from multifunctional magneto-plasmonic NRs for each miRNA expression from the different cross-sections of brain tissue explants (i–iv). Nucleus (Hoechst, blue), GFAP (Alexa Fluor 488, green), and TuJ1 (Alexa Fluor 647, red) (scale bar =  $100 \mu m$ ) (i–iv). (The error bars represent mean  $\pm$  SD; n = 3, \*\*p < 0.01 by one-way ANOVA with Tukey's post hoc test.)

temperature. At elevated temperature (65 °C), the MB strand unfolded, and a clear and strong fluorescence signal at 520 nm was observed. The cleavage of MB from the magneto-plasmonic NR surface using exonuclease I (ExoI), on the other hand, showed 15-fold less fluorescence signal compared to the unfolded state. These results clearly demonstrated the robustness of the MEF effect obtained by our magneto-plasmonic NR-based exosomal miRNA detection method. We further optimized the enhancement of the fluorescence signal by testing different lengths of MBs from 19 to 49 bps (6.5 to 16.7 nm in length). Due to the quenching and MEF effect, MB-25 (25 bps, 8.5 nm) showed the strongest fluorescence signal [Figure 3c], while the fluorescence signal was quenched for the shorter MB and significantly decreased for the longer MBs.

Next, we validated the specificity of our multifunctional magneto-plasmonic NR-based detection method by examining the synthetic miR-124-targeting MB. Using a solution-based assay, we observed a strong fluorescence signal from the hybridization between the synthesized miR-124-targeting MB and complementary DNA sequences (positive control). However, when miR-124-targeting MB interacted with single-base-pair-mismatched DNA and miRNA-67 (miR-67) DNA sequence (negative control), little to no fluorescence signals were observed [Figure 3d and Table S1]. In addition, our MB-functionalized magneto-plasmonic NR-based miRNA detection method showed good linearity ( $R^2 = 0.98$ ) at different concentrations (ranging from 1 pM to 1  $\mu$ M) of the complementary DNA sequence of miR-124 [Figure 3e], which

agreed with previously reported miRNA assays.<sup>34–36</sup> Altogether, we showed that our multicomponent magneto-plasmonic NRs based on the miRNA detection method were highly selective and sensitive and can quantify the concentrations of miR-124 in exosomes secreted by cells.

Nondestructive, Selective, and Sensitive Characterization of Neurogenesis of hiPSC-NSCs through Immuno-Magnetically Concentrated Exosomal miRNA Detection. After confirming the selectivity and sensitivity of our magneto-plasmonic NRs miRNA detection platform, we then applied our nondestructive detection technique to demonstrate its feasibility for characterizing the neuronal differentiation of hiPSC-NSCs [Figure 4a]. For this purpose, we first confirmed the neuronal differentiation of hiPSC-NSCs through immunocytochemistry staining of Nestin and neuron-specific class III  $\beta$ tubulin (TuJ1), the representative markers of neural stem cells (NSCs) and differentiated neurons, respectively. 37,38 As shown in Figure 4b, we observed a clear TuJ1 expression (D8 and D22) in cells that have undergone neuronal differentiation, while the undifferentiated hiPSC-NSCs cells (D1 and D4) showed Nestin expression only, without any significant TuJ1 expression. Additionally, we conducted reverse transcription polymerase chain reaction (RT-PCR) over the differentiation period (3 weeks) and found that the expression trend of miR-124 was similar to that of Tuj1 mRNA expression. The expression level (from D1 to D22) of miR-124 showed a time-dependent increase and saturation as the neuronal differentiation proceeded [Figure 4c]. On the basis of the well-correlated

expressions of miR-124 with neuronal marker TuJ1, we concluded that the monitoring of miR-124 expression was a reliable method to characterize neuronal differentiation of hiPSC-NSCs.

To effectively capture and isolate exosomes, we attached anti-CD63 IgG antibody, one of many general membrane markers (CD63, CD9, etc.), on the outer membrane of the exosome 15,16 on the surface of the ferromagnetic Ni block of the magnetoplasmonic NRs for the immunomagnetic isolation and concentration of the targeted exosomes. Specifically, we were able to collect cell culture medium throughout the neuronal differentiation period (3 weeks) of hiPSC-NSCs and immunomagnetically isolate and concentrate exosomes to analyze exosomal miR-124 expression in a nondestructive, selective, and sensitive manner [Figure 4a]. The capture and concentration of exosomes by the multifunctional magneto-plasmonic NRs were verified through two independent methods: scanning electron microscope (SEM) analysis and a sandwich assay based on 3,3',5,5'-tetramethylbenzidine (TMB) reaction. 15 From the SEM analysis, we confirmed the surface of the ferromagnetic Ni block region, functionalized with exosomes capturing anti-CD63 antibody, of the magneto-plasmonic NRs was densely covered with cell-derived exosomes, demonstrating the high capture and isolation properties [Figure 4d]. Additionally, the TMB sandwich assay also showed a clear absorbance signal, while no observable signal was obtained from magnetoplasmonic NRs without the functionalization of anti-CD63 antibody [Figure 4e]. After immunomagnetic isolation of exosomes, concentrated exosomes were lysed to release the encapsulated components including miRNAs. As shown in Figure 4f, no observable fluorescence signal was registered by the undifferentiated hiPSC-NSCs (D1). In contrast, a distinct fluorescence signal began to be prominent starting from the premature (D4) time point and saturated at the mature (D15) neuron formation [Figure 4f]. Furthermore, the results collected from our nondestructive exosomal miRNA detection method were in agreement with the results collected by the cell lysing traditional RT-PCR technique for characterizing neuronal differentiation [Figure 4c]. In addition, owing to the specificity of our designed MB to miR-124, our multifunctional magnetoplasmonic NRs showed the ability to selectively and sensitively distinguish neurons from other types of ectoderm cells including hiPSC-NSCs and astrocytes, as well as endoderm and mesoderm cells [Figure 4g].

Nondestructive Characterization of Neural Cell Distribution in the Explanted Brain Tissues. With the encouraging results from the above studies thus far, we set forth to explore the practicability of applying our magnetoplasmonic NR in a more complex, heterogeneous system such as biological tissue. Since the supporting cells of the brain are predominantly astrocytes, we designed an additional miRNA-449a (miR-449a) MB to specifically target astrocytes [Table S1].<sup>39,40</sup> In this proof-of-concept demonstration, we characterized the distribution of cell types in brain tissue [Figure 5a]. Similar to our previous optimization process, we first verified the correlation between cell-type-specific exosomal miRNAs in neurons and astrocytes separately using miR-124- and miR-449a-specific MB-functionalized magneto-plasmonic NRs [Figure 5b and c]. As expected, neurons showed a fluorescent signal from miR-124-specific magneto-plasmonic NRs only, and astrocytes showed a fluorescent signal with miR-449a-specific magnetic-gold NRs only. The fluorescent signals obtained from neurons- and astrocytes-derived exosomes were positively

correlated to the number of cells in the cell culture conditions [Figure S3a and b]. Through the collected ratiometric fluorescence signals among cocultured neurons and astrocytes at various ratios [Figure S3c], we proved that our non-destructive, selective, and sensitive multifunctional magneto-plasmonic NR-based detection method was a reliable and quantitative exosomal miRNA detection method.

Owing to the modular, interchangeable targeting moieties (e.g., target specific MB and antibody) and the nondestructive, selective, and sensitive neurogenesis characterization of our magneto-plasmonic NRs, we then analyzed the different cell populations of mouse brain tissue explants [Figure 5a]. In this ex vivo rodent model, brain tissues were dissected from a mouse (postnatal day 4) and cultured on Matrigel-coated plates. During this step, brain tissue sections from different regions of the brain such as the cerebral cortex, cerebellum, and the rest of brain adhered on Matrigel-coated plates. After 3 days of cultivation, the cell culture medium was collected for analysis, and the tissues were fixed with formaldehyde solution. The distribution of neurons and astrocytes was characterized through immunocytochemistry staining of the neuron-specific marker (TuJ1) and glial fibrillary acidic protein (GFAP), representative markers of neurons and astrocytes, respectively. The populations of neurons and astrocytes varied from each brain tissue sample following the glia to neuron ratios reported for rodents depending on the sections of the brain (such as cerebral cortex, cerebellum, and the rest of the brain). 41 Using our magneto-plasmonic NRs-based exosomal miRNA detection method, we also showed correlative fluorescent signal ratios on each brain tissue sample with immunostaining results [Figure 5d]. These results demonstrated the feasibility of our magnetoplasmonic NRs to verify the distribution ratio of neurons and astrocytes in real tissues in a nondestructive, selective, and sensitive manner. Although these results were obtained from brain tissue explants, we firmly believe our innovative exosomal miRNA detection method can be extended to the actual clinical settings for patients who suffer neurodegenerative diseases and injuries as well.

# **CONCLUSIONS**

In conclusion, we have successfully developed an innovative exosomal miRNA detection method to monitor stem cell neurogenesis in a nondestructive, selective, and sensitive manner using multifunctional magneto-plasmonic NRs by integrating (i) a central Ni component to immunomagnetically isolate and concentrate exosomes and (ii) two end-capping Au components to detect captured miRNA expression via MB with an MEF effect. We further explored a potential realistic application of our multifunctional magneto-plasmonic NRs by characterizing heterogeneous populations of brain tissue explants. We will further investigate the versatility of our multifunctional magneto-plasmonic NRs-based miRNA analysis such as subtype-specific neurons (dopaminergic, glutamatergic, etc.) detection for more clinically relevant applications. Moreover, by avoiding any destructive analysis processes such as cell lysis and cell fixation, our multifunctional magneto-plasmonic NR-based sensing method can lead to a breakthrough in preclinical research such as the transplantation of differentiated stem cells. We believe that our multifunctional magnetoplasmonic NRs-based characterization method will not only advance stem cell differentiation assays by providing a practical, nondestructive monitoring tool but also promote the realization of stem cell-based therapies and advanced diagnostics.

## **METHODS**

Generation of Magneto-Plasmonic Nanorods via Electrodeposition. The generation method for magnetic-gold nanorods was adopted from previous reports.<sup>42–44</sup> Briefly, a thin layer of silver (approximately, 300 nm) was evaporated on one side of the AAO template (Anodisk 13, Whatman) by physical vapor deposition as a conducting layer. By providing electrical contact with aluminum foil in the Teflon cell with a Ag layer on one side of the AAO template, the AAO template served as a working electrode in an electrochemical setup. In addition, a Ag/AgCl and a Pt wire served as the reference and counter electrode to form a three-electrode configuration. To block the irregular branch part of the AAO nanopores, Ag was predeposited into AAO by a commercial plating solution at -0.95 V ( $\nu s$  Ag/AgCl). In order to synthesize the magneto-plasmonic nanorods, approximately 250 nm of both Ni and Au components are sequentially deposited by a commercial plating solution at -0.95 V (vs Ag/AgCl). The desired configuration and length of each block of nanorods were controlled by the type of plating solution selected and the depositing Coulomb value applied. Specifically, ca. 0.07 Coulomb was needed for the growth of a 250 nm block of Au, and ca. 0.20 Coulomb was needed for the growth of a 250 nm block of Ni. The lengths of Au and Ni components were measured from SEM images obtained by cross-deposition of Au and Ni on an AAO template with varying charge Coulombs. The correlation between Coulomb values applied for electrochemical growth of each component (Au and Ni) was characterized by FE-SEM (Sigma, Zeiss, Germany). Twenty random components from each condition were used to measure the length of each component [Figure S1]. The Ag layer was etched with a 4:1:1 ratio mixture of methanol (CH<sub>3</sub>OH), hydrogen peroxide (H<sub>2</sub>O<sub>2</sub>) (30% vol/vol), and ammonium hydroxide (NH<sub>4</sub>OH) (28% in H<sub>2</sub>O), respectively. 44 The AAO template was then completely removed by 3 M NaOH for 50 min. 43 The resulting samples were rinsed with distilled water and visualized with an FE-SEM on an indium tin oxide-coated glass substrate.

Preparation of Multifunctional Magneto-Plasmonic Nanorods. Each component of magneto-plasmonic NRs was functionalized with a FAM-tagged MB against miR-124 and antibody against CD63, respectively [Table S1]. First, presynthesized magneto-plasmonic NRs were washed with phosphate-buffered saline (PBS) three times using centrifugation (centrifuge 5415R; Eppendorf, Germany). To selectively functionalize the surface of the Au component only, magnetic-gold NRs were incubated with thiol group-functionalized MB (final concentration 10  $\mu$ M) [Table S1] and 1,4-dithiothreitol (C<sub>4</sub>H<sub>10</sub>O<sub>2</sub>S<sub>2</sub>) (final concentration 100 µM) for 8 h at 4 °C to promote covalent bonding between Au and thiol. After functionalizing the Au block, magnetic-gold NRs were washed with PBS three times and incubated with the anti-CD63 antibody (final concentration range from 10 µg/mL) to functionalize the Ni component as well. After an 8 h incubation period at 4 °C, 3% bovine serum albumin (BSA) was added to the mixed solution to stabilize the multifunctional magneto-plasmonic NRs.

Fluorescence Measurements and Experimental Setup. Anti-CD63 antibody and FAM-tagged miR-124-targeting MB-modified multifunctional magneto-plasmonic NRs (20 mg/mL) were mixed with cell culture medium (1 mL) which are obtained during neuronal differentiation of human stem cells. After 30 min, magneto-plasmonic NRs were isolated under magnetic field (BioMag, Polyscience Inc.) and resuspended in a transparent 96-well plate with PBS with 0.1% Tween 20 (100  $\mu$ L). The fluorescence spectra were recorded with an excitation of 490 nm and emission of 520 nm at 25 °C using a 96-well plate reader (Infinite M200pro, TECAN Group, Ltd., Switzerland).

Finite-Difference Time-Domain Simulation. To study the metal-enhanced fluorescence surrounding the multicomponent magneto-plasmonic NRs, electromagnetic field enhancement surrounding the magneto-plasmonic NRs was simulated and calculated using the FDTD package provided by Lumerical. To match the fluorescence excitation wavelength, a plane wave light source model with a single wavelength of 490 nm was introduced. Magneto-plasmonic NRs with a diameter of 278 nm and heights of 248, 250, and 248 nm for each section were used to be consistent with the nanorods we synthesized. Re (index) and Im (index) were used from the materials library without further modifications. To simulate light from different directions, two

models were calculated: one model with the light source vertical to the longitudinal axis of the NR and the other model with the light source horizontal to the longitudinal axis of the NR. In the vertical model, the light source was placed at 400 nm on top of the NR, while in the horizontal model the distance is kept at 500 nm. A mesh size of 4 nm was utilized for all simulations, and the media surrounding the nanorods were set as a vacuum. Monitors were set at different locations of NRs with fixed wavelengths of 490 nm. The electromagnetic field was calculated and plotted in the heat map of  $E/E_0$  and summarized in Figure 3b.

Cell Culture and Differentiation. The human induced pluripotent stem cell-derived neural stem cells were maintained in mixture of neural basal medium (Gibco) and DMEM/F12 (Gibco) (50:50 ratio) supplemented with 0.5% N2 (Gibco), 0.5% B27, and 20 ng/mL FGF basic (Fibroblast growth factor-basic, PeproTech), respectively. All cells were maintained at 37 °C in a humidified incubator with 5% CO2. To differentiate cells, hiPSC-NSCs were seeded on Matrigel (Life Technologies)-precoated plates (300 000 cells/well in a six-well plate) 24 h prior to experimentation. After 1 day of cultivation to promote cell attachment and spreading, the fresh hiPSC-NSC media without FGF basic (differentiation media) was treated to stop proliferation and induce neuronal differentiation. The medium was changed with fresh differentiation media every 3 to 4 days during the differentiation. For consistency, all experiments were carried out on cells between three passage differences. Human mesenchymal stem cells (American CryoStem) were maintained in Alpha MEM (Lglutamine) supplemented with 10% SCM141 (PLTMax human platelet lysate), 30 mg of heparin sodium salt, and 1% penicillin/streptomycin (Gibco). The human cerebral microvascular endothelial cells were cultured in the human endothelial cell culture medium (Cell Applications, Inc.) supplemented with 5% fetal bovine serum (FBS), penicillin (100 units/mL), streptomycin (100  $\mu$ g/mL), 1.4  $\mu$ M hydrocortisone, 5  $\mu$ g/mL ascorbic acid, 10 mM HEPES, and 1 ng/ mL basic fibroblast growth factor (bFGF). The astrocytes were maintained in the astrocyte culture medium (Sciencell) with 10% FBS, penicillin (100 units/ml), and streptomycin (100  $\mu$ g/mL). Human dermal fibroblasts were cultivated in fibroblast growth medium (Cell Applications, Inc.). For the collection of exosomes from each of the cell lines,  $3 \times 10^6$  cells were seeded in a six-well plate, and each media were collected after 3 days from the seeding. ReN cells (human neural progenitor cell line) were obtained from Merck and maintained in DMEM/F12 (Gibco) supplemented with 1% L-glutamine (200 nM, Invitrogen), 2% B27, 20 ng/mL heparin (Sigma-Aldrich), gentamycin (10 µg/mL), 0.1% bFGF (Sigma-Aldrich), and 0.1% EGF (epidermal growth factor, Sigma-Aldrich), respectively. In the case of the ReN cell differentiation, a similar protocol was used with hiPSC-NSCs. ReN cells were seeded on Matrigel-precoated plates (2 000 000 cells/well for sixwell plate) 24 h prior to experimentation. After 1 day of cultivation to promote cell attachment and spreading, the fresh ReN cell media without bFGF basic (differentiation media) was treated to stop proliferation and induce neuronal differentiation. ReN cells and astrocytes were cocultured in one dish and induced neural differentiation. Both were maintained in a mixture of DMEM/F12 (Gibco) and astrocyte culture medium (1:1 ratio) with all supplements. Total seeding numbers of cells were  $2.0 \times 10^6$ , corresponding to 1.9/1.4/1.1/1.14:1/9:1 ratios for ReN cells and astrocytes, respectively. ReN cells and astrocytes were seeded on Matrigel-precoated plates 24 h prior to experimentation. After 1 day of cultivation to promote cell attachment and spreading, the fresh mixture of cell media without bFGF basic was treated to stop proliferation and induce neuronal differentiation. The medium was changed with fresh differentiation media every 3 to 4 days during the differentiation. The culture media was collected 10 days after the induction of neural differentiation. Then, the media were centrifuged at 2000 rpm for 5 min to separate the cell debris. For consistency, all experiments were carried out on cells between passages 3 and 5.

**Immunocytochemistry.** To study the extent of neuronal differentiation, cells and explanted brain tissue were washed with PBS (pH 7.4) and fixed with 4% formaldehyde solution for 10 min at room temperature, followed by washing with PBS three times. Then, cells

were permeabilized with 0.1% Triton X-100 in PBS for 10 min, and nonspecific binding was blocked with 5% normal goat serum (NGS) (eLife Technologies) in PBS for 1 h at room temperature. The primary rabbit antibody against Nestin (1:200 dilution, Invitrogen) and primary mouse antibody against TuJ1 (1:200 dilution, Biolegend) were used for the cells. Moreover, the primary rabbit antibody against GFAP (1:200 dilution, Invitrogen) and primary mouse antibody against TuJ1 (1:200 dilution, Biolegend) were used for the explanted brain tissues. Following the manufacturer's protocol, the fixed samples were incubated overnight at 4 °C in a solution of this antibody in PBS containing 1% BSA and 0.3% Triton X-100. After washing three times with PBS, the samples were incubated for 1 h at room temperature in a solution of anti-rabbit secondary antibody labeled Alexa Fluor 488 (1:100, Life Technologies), anti-mouse secondary antibody labeled with Alexa Fluor 647 (1:100, Life Technologies), and Hoechst (3  $\mu$ g/ mL, Life Technologies) to stain nuclei in PBS containing 1% NGS and 0.3% Triton X-100. After washing three times, all the samples were imaged using a Nikon T2500 inverted fluorescence microscope.

**Gene Expression Analysis.** Gene expression level was analyzed by quantitative reverse transcription PCR from total RNA extracted from cells by a TRIzol reagent (Invitrogen, MA, USA). The total RNA (1  $\mu$ g) was reverse transcribed to cDNA using the SuperScript III first-strand synthesis system (Invitrogen, MA, USA) following the manufacturer's protocol. Subsequently, quantitative PCR was performed on a StepOnePlus real-time PCR system (Applied Biosystems, MA, USA) using a SYBR Green PCR master mix (Applied Biosystems) with the gene-specific primers, listed in Table S2. The standard cycling conditions were used for all PCR reactions with a melting temperature of 60 °C. All the measurements were run in triplicate. The gene expression level was reported relative to the endogenous control gene, GAPDH.

Quantification of Intracellular miRNA Expression. The intracellular miRNA expression was quantified throughout differentiation (21 days). At each time point, the total RNA, including miRNA, was extracted from cultured cells using the miRNeasy micro kit (Qiagen, MD, USA) following the manufacturer's protocol. The firststrand cDNA was synthesized from total RNA (50 ng) using a universal reverse transcription reaction system offered in the miRCURY LNA RT kit (Qiagen). The as-synthesized cDNA template was diluted 60 times prior to real-time PCR amplification on a StepOnePlus real-time PCR System (Applied Biosystems, MA). Each real-time PCR was carried out in a miRCURY LNA miRNA PCR system (Qiagen) in a  $10\,\mu\text{L}$  reaction with 3 µL of cDNA, 5 µL of 2× miRCURY SYBR Green master mix, and the miRNA-specific PCR assays (primers): hsa-miR-124-5p as miR-124-specific primers and hsa-miR-103a-3p as the endogenous control. The two-step cycling conditions were performed as follows: Initiation activation at 95 °C for 2 min, 40 cycles of denaturation at 95  $^{\circ}$ C for 10 s, and combined annealing/extension at 56  $^{\circ}$ C for the 60 s. The resulting CT values were normalized and reported in fold changes relative to the endogenous control (miR-103a-3p). All measurements were repeated three times.

**Confirmation of Extraction and Concentration of Exosomes** via Magneto-Plasmonic Nanorods Based on HRP-TMB Reaction. Anti-CD63- and miR-124-targeting MB-functionalized magnetoplasmonic NRs (20 mg/mL) were mixed with cell culture medium (1 mL), which were attained during neuronal differentiation of hiPSC-NSCs. After 30 min, NRs were isolated under a magnetic field and resuspended with the anti-CD9-HRP antibody (Santa Cruz Biotechnology, Inc.) in PBS (final concentration  $10 \,\mu g/mL$ ). After 30 min, multifunctional magneto-plasmonic NRs were repeatedly isolated under magnetic field and resuspend with PBS three times for separation of unbound anti-CD9-HRP. After the washing step, TMB (MP Biomedicals, Inc.) was added to the multifunctional magnetoplasmonic NR solution for 30 min. The UV/vis absorbance value was obtained at 650 nm using a 96-well plate reader (Infinite M200pro, TECAN Group, Ltd., Switzerland). In addition, to validate the exosome isolation efficiency and selectivity of our system, we compared our immunomagnetic isolation method to the most widely used "ultracentrifugation" method (centrifugation with 100000g for 1 h at 4 °C, Optima XE-90 with SW41 Ti rotor; Beckman Coulter, USA) [Figure

S4a]. We measured the overall lipid concentrations (lipid assay kit, Abcam, UK) from the collected exosomes after the isolation procedures. As shown, the isolation efficiency of the immunomagnetic (IM) isolation method (95.8  $\pm$  10.3%) was comparable to the ultracentrifugation (UC) method at the condition of 100 mg/mL of multifunctional magneto-plasmonic NRs for 1 mL of biological fluid [Figure S4b]. We also performed the bicinchoninic acid (BCA) assay to measure the overall protein concentration from the collected exosomes after the isolation procedures to validate the specificity of exosome isolation methods (UC and IM) [Figure S4c]. 45 Compared to lipid quantification, protein quantification (BCA assay) (89.3 ± 5.1%) showed a large signal difference between UC and IM. These results could be due to the presence of nonexosomal protein impurities such as aggregated proteins and ribonuclear protein particles obtained from the ultracentrifugation method. <sup>17</sup> As a result, the overall exosome isolation efficiency of our platform was comparable to the most widely used isolation method "ultracentrifugation". In addition, our platform has the advantage of improved selectivity from the attached antibody specific to exosomes on the surface of multifunctional magnetoplasmonic NRs.

Nondestructive Characterization of Neural Cell Distribution in the Explanted Brain Tissues. CD1 postnatal day 4 (P4) mice brain tissue was dissected and maintained in a mixture of neural basal medium (Gibco) and DMEM/F12 (Gibco) (50:50 ratio) supplemented with 0.5% N2 (Gibco) and 0.5% B27, respectively. Brain tissue was maintained at 37 °C in a humidified incubator with 5% CO<sub>2</sub>. After 1 day of cultivation, nonadhered tissue was removed, and the fresh medium was introduced. The medium was changed with fresh differentiation media every 3 to 4 days during the differentiation. For the collection of the exosomes, media were collected after 3 days from the explant. The cultured media were then centrifuged at 2000 rpm for 5 min to separate the cell debris.

## **ASSOCIATED CONTENT**

## S Supporting Information

The Supporting Information is available free of charge on the ACS Publications website at DOI: 10.1021/acsnano.9b01875.

Supplementary figures and tables (PDF)

# **AUTHOR INFORMATION**

## **Corresponding Authors**

\*E-mail: jwchoi@sogang.ac.kr.

\*E-mail: kblee@rutgers.edu. Web: http://kblee.rutgers.edu/.

#### ORCID ®

Jin-Ho Lee: 0000-0002-5877-0222 Jin-Ha Choi: 0000-0002-1632-9586

Sy-Tsong Dean Chueng: 0000-0002-1447-5491 Thanapat Pongkulapa: 0000-0003-0678-1736

Letao Yang: 0000-0002-0572-9787 Hyeon-Yeol Cho: 0000-0003-1897-1166 Jeong-Woo Choi: 0000-0003-0100-0582 Ki-Bum Lee: 0000-0002-8164-0047

# **Author Contributions**

J.-H.L. and J.-H.C. contributed equally.

#### Notes

The authors declare no competing financial interest.

## **ACKNOWLEDGMENTS**

K.-B.L. acknowledges the partial financial support from the NIH R21 (1R21NS085569 and R21AR071101), NIH R01 (1R01DC016612-01, 3R01DC016612-01S1, and 3R01DC016612-02S1), New Jersey Commission on Spinal Cord Research [CSCR17IRG010 and CSCR16ERG019], NSF [CHE-1429062 and CBET-1803517], and the ACS New

Directions Award (PRF# 55869-ND10). J.-W.C. acknowledges partial financial support from the NRF (2019R1A2C3002300 and 2016R1A6A1A03012845) funded by MSIP and the ME of Korea. We are also grateful to C. Rathnam, Y. Ying, and K. Kwan for their kind support and valuable discussions on brain explant experiments.

#### **REFERENCES**

- (1) Ascherio, A.; Schwarzschild, M. A. The Epidemiology of Parkinson's Disease: Risk Factors and Prevention. *Lancet Neurol.* **2016**. *15*. 1257–1272.
- (2) Logroscino, G.; Piccininni, M.; Marin, B.; Nichols, E.; Abd-Allah, F.; Abdelalim, A.; Alahdab, F.; Asgedom, S. W.; Awasthi, A.; Chaiah, Y.; Daryani, A.; Do, H. P.; Dubey, M.; Elbaz, A.; Eskandarieh, S.; Farhadi, F.; Farzadfar, F.; Fereshtehnejad, S. M.; Fernandes, E.; Filip, I.; et al. Global, Regional, and National Burden of Motor Neuron Diseases 1990–2016: A Systematic Analysis for the Global Burden of Disease Study 2016. *Lancet Neurol.* 2018, 17, 1083–1097.
- (3) Trounson, A.; DeWitt, N. D. Pluripotent Stem Cells Progressing to the Clinic. *Nat. Rev. Mol. Cell Biol.* **2016**, *17*, 194–200.
- (4) Fox, I. J.; Daley, G. Q.; Goldman, S. A.; Huard, J.; Kamp, T. J.; Trucco, M. Stem Cell Therapy. Use of Differentiated Pluripotent Stem Cells as Replacement Therapy for Treating Disease. *Science* **2014**, *345*, 1247391.
- (5) Lee, A. S.; Tang, C.; Rao, M. S.; Weissman, I. L.; Wu, J. C. Tumorigenicity as a Clinical Hurdle for Pluripotent Stem Cell Therapies. *Nat. Med.* **2013**, *19*, 998.
- (6) Shi, Y.; Inoue, H.; Wu, J. C.; Yamanaka, S. Induced Pluripotent Stem Cell Technology: a Decade of Progress. *Nat. Rev. Drug Discovery* **2017**, *16*, 115.
- (7) Chen, K. G.; Mallon, B. S.; McKay, R. D.; Robey, P. G. Human Pluripotent Stem Cell Culture: Considerations for Maintenance, Expansion, and Therapeutics. *Cell Stem Cell* **2014**, *14*, 13–26.
- (8) Dimmeler, S.; Ding, S.; Rando, T. A.; Trounson, A. Translational Strategies and Challenges in Regenerative Medicine. *Nat. Med.* **2014**, 20, 814–821.
- (9) Goodwin, H. S.; Bicknese, A. R.; Chien, S. N.; Bogucki, B. D.; Quinn, C. O.; Wall, D. A. Multilineage Differentiation Activity by Cells Isolated from Umbilical Cord Blood: Expression of Bone, Fat, and Neural Markers. *Biol. Blood Marrow Transplant.* **2001**, *7*, 581–588.
- (10) Lee, J. H.; Choi, H. K.; Yang, L.; Chueng, S. T. D.; Choi, J. W.; Lee, K. B. Nondestructive Real-Time Monitoring of Enhanced Stem Cell Differentiation Using a Graphene-Au Hybrid Nanoelectrode Array. *Adv. Mater.* **2018**, *30*, 1802762.
- (11) Zhang, W.; Kim, P. J.; Chen, Z.; Lokman, H.; Qiu, L.; Zhang, K.; Rozen, S. G.; Tan, E. K.; Je, H. S.; Zeng, L. MiRNA-128 Regulates the Proliferation and Neurogenesis of Neural Precursors by Targeting PCM1 in the Developing Cortex. *eLife* **2016**, *5*, No. e11324.
- (12) Yao, B.; Christian, K. M.; He, C.; Jin, P.; Ming, G. L.; Song, H. Epigenetic Mechanisms in Neurogenesis. *Nat. Rev. Neurosci.* **2016**, *17*, 537–549.
- (13) Ratajczak, J.; Miekus, K.; Kucia, M.; Zhang, J.; Reca, R.; Dvorak, P.; Ratajczak, M. Z. Embryonic Stem Cell-Derived Microvesicles Reprogram Hematopoietic Progenitors: Evidence for Horizontal Transfer of mRNA and Protein Delivery. *Leukemia* 2006, 20, 847–856.
- (14) Vlassov, A. V.; Magdaleno, S.; Setterquist, R.; Conrad, R. Exosomes: Current Knowledge of Their Composition, Biological Functions, and Diagnostic and Therapeutic Potentials. *Biochim. Biophys. Acta, Gen. Subj.* **2012**, *1820*, 940–948.
- (15) Thery, C.; Ostrowski, M.; Segura, E. Membrane Vesicles as Conveyors of Immune Responses. *Nat. Rev. Immunol.* **2009**, *9*, 581–593.
- (16) Im, H.; Shao, H.; Park, Y. I.; Peterson, V. M.; Castro, C. M.; Weissleder, R.; Lee, H. Label-Free Detection and Molecular Profiling of Exosomes with a Nano-Plasmonic Sensor. *Nat. Biotechnol.* **2014**, *32*, 490–495.

(17) Shao, H.; Im, H.; Castro, C. M.; Breakefield, X.; Weissleder, R.; Lee, H. New Technologies for Analysis of Extracellular Vesicles. *Chem. Rev.* **2018**, *118*, 1917–1950.

- (18) Huang, X.; Yuan, T.; Tschannen, M.; Sun, Z.; Jacob, H.; Du, M.; Liang, M.; Dittmar, R. L.; Liu, Y.; Liang, M.; Kohli, M.; Thibodeau, S. N.; Boardman, L.; Wang, L. Characterization of Human Plasma-Derived Exosomal RNAs by Deep Sequencing. *BMC Genomics* **2013**, *14*, 319.
- (19) Lund, E.; Guttinger, S.; Calado, A.; Dahlberg, J. E.; Kutay, U. Nuclear Export of MicroRNA Precursors. *Science* **2004**, *303*, 95–98.
- (20) Lai, E. C. Micro RNAs are Complementary to 3' UTR Sequence Motifs that Mediate Negative Post-Transcriptional Regulation. *Nat. Genet.* 2002, 30, 363
- (21) Valadi, H.; Ekstrom, K.; Bossios, A.; Sjostrand, M.; Lee, J. J.; Lotvall, J. O. Exosome-Mediated Transfer of mRNAs and MicroRNAs is a Novel Mechanism of Genetic Exchange Between Cells. *Nat. Cell Biol.* **2007**, *9*, 654–659.
- (22) van Niel, G.; D'Angelo, G.; Raposo, G. Shedding Light on the Cell Biology of Extracellular Vesicles. *Nat. Rev. Mol. Cell Biol.* **2018**, *19*, 213–228
- (23) Tkach, M.; Thery, C. Communication by Extracellular Vesicles: Where We Are and Where We Need to Go. *Cell* **2016**, *164*, 1226–1232.
- (24) Pegtel, D. M.; Cosmopoulos, K.; Thorley-Lawson, D. A.; van Eijndhoven, M. A.; Hopmans, E. S.; Lindenberg, J. L.; de Gruijl, T. D.; Wurdinger, T.; Middeldorp, J. M. Functional Delivery of Viral miRNAs via Exosomes. *Proc. Natl. Acad. Sci. U. S. A.* **2010**, *107*, 6328–6333.
- (25) Greening, D. W.; Xu, R.; Ji, H.; Tauro, B. J.; Simpson, R. J., A Protocol for Exosome Isolation and Characterization: Evaluation of Ultracentrifugation, Density-Gradient Separation, and Immunoaffinity Capture Methods. In *Proteomic Profiling*; Springer, 2015; pp 179–209.
- (26) Melo, S. A.; Luecke, L. B.; Kahlert, C.; Fernandez, A. F.; Gammon, S. T.; Kaye, J.; LeBleu, V. S.; Mittendorf, E. A.; Weitz, J.; Rahbari, N.; Reissfelder, C.; Pilarsky, C.; Fraga, M. F.; Piwnica-Worms, D.; Kalluri, R. Glypican-1 Identifies Cancer Exosomes and Detects Early Pancreatic Cancer. *Nature* **2015**, *523*, 177–182.
- (27) Taylor, D. D.; Zacharias, W.; Gercel-Taylor, C. Exosome Isolation for Proteomic Analyses and RNA Profiling. In *Serum/Plasma Proteomics*; Springer, 2011; pp 235–246.
- (28) Lee, S. A.; Liu, L.; Kim, S. K.; Park, S. Tri-Component Gold—Nickel—Silver Nanorods Leading to Multiple Surface Plasmon Bands. *J. Phys. Chem. C* **2012**, *116*, 18388—18393.
- (29) Papagiannakopoulos, T.; Kosik, K. S. MicroRNA-124: Micromanager of Neurogenesis. *Cell Stem Cell* **2009**, *4*, 375–376.
- (30) Aslan, K.; Gryczynski, I.; Malicka, J.; Matveeva, E.; Lakowicz, J. R.; Geddes, C. D. Metal-Enhanced Fluorescence: An Emerging Tool in Biotechnology. *Curr. Opin. Biotechnol.* **2005**, *16*, 55–62.
- (31) Kuhn, S.; Hakanson, U.; Rogobete, L.; Sandoghdar, V. Enhancement of Single-Molecule Fluorescence Using a Gold Nanoparticle as an Optical Nanoantenna. *Phys. Rev. Lett.* **2006**, *97*, 017402.
- (32) Chen, Y.; Munechika, K.; Ginger, D. S. Dependence of Fluorescence Intensity on the Spectral Overlap Between Fluorophores and Plasmon Resonant Single Silver Nanoparticles. *Nano Lett.* **2007**, *7*, 690–696.
- (33) Li, M.; Cushing, S. K.; Wu, N. Plasmon-Enhanced Optical Sensors: A Review. *Analyst* **2015**, *140*, 386–406.
- (34) Qiu, X.; Hildebrandt, N. Rapid and Multiplexed MicroRNA Diagnostic Assay Using Quantum Dot-Based Forster Resonance Energy Transfer. ACS Nano 2015, 9, 8449–8457.
- (35) Graybill, R. M.; Bailey, R. C. Emerging Biosensing Approaches for microRNA Analysis. *Anal. Chem.* **2016**, *88*, 431–450.
- (36) Mahdiannasser, M.; Karami, Z. An Innovative Paradigm of Methods in microRNAs Detection: Highlighting DNAzymes, the Illuminators. *Biosens. Bioelectron.* **2018**, *107*, 123–144.
- (37) Gage, F. H.; Coates, P. W.; Palmer, T. D.; Kuhn, H. G.; Fisher, L. J.; Suhonen, J. O.; Peterson, D. A.; Suhr, S. T.; Ray, J. Survival and Differentiation of Adult Neuronal Progenitor Cells Transplanted to the Adult Brain. *Proc. Natl. Acad. Sci. U. S. A.* 1995, 92, 11879–11883.

(38) Cheng, L.; Hu, W.; Qiu, B.; Zhao, J.; Yu, Y.; Guan, W.; Wang, M.; Yang, W.; Pei, G. Generation of Neural Progenitor Cells by Chemical Cocktails and Hypoxia. *Cell Res.* **2014**, *24*, 665–679.

- (39) Jovicic, A.; Roshan, R.; Moisoi, N.; Pradervand, S.; Moser, R.; Pillai, B.; Luthi-Carter, R. Comprehensive Expression Analyses of Neural Cell-Type-Specific miRNAs Identify New Determinants of the Specification and Maintenance of Neuronal Phenotypes. *J. Neurosci.* **2013**, 33, 5127–5137.
- (40) Rao, V. T.; Ludwin, S. K.; Fuh, S. C.; Sawaya, R.; Moore, C. S.; Ho, M. K.; Bedell, B. J.; Sarnat, H. B.; Bar-Or, A.; Antel, J. P. MicroRNA Expression Patterns in Human Astrocytes in Relation to Anatomical Location and Age. *J. Neuropathol. Exp. Neurol.* **2016**, *75*, 156–166.
- (41) Herculano-Houzel, S. The Glia/Neuron Ratio: How it Varies Uniformly Across Brain Structures and Species and What that Means for Brain Physiology and Evolution. *Glia* **2014**, *62*, 1377–1391.
- (42) Martin, C. R. Nanomaterials: A Membrane-Based Synthetic Approach. *Science* **1994**, *266*, 1961–1966.
- (43) Lee, S. A.; Liu, L.; Kim, S. K.; Park, S. Tri-Component Gold–Nickel–Silver Nanorods Leading to Multiple Surface Plasmon Bands. *J. Phys. Chem. C* **2012**, *116*, 18388–18393.
- (44) Banholzer, M. J.; Qin, L.; Millstone, J. E.; Osberg, K. D.; Mirkin, C. A. On-Wire Lithography: Synthesis, Encoding and Biological Applications. *Nat. Protoc.* **2009**, *4*, 838–848.
- (45) Rupert, D. L.; Lasser, C.; Eldh, M.; Block, S.; Zhdanov, V. P.; Lotvall, J. O.; Bally, M.; Hook, F. Determination of Exosome Concentration in Solution Using Surface Plasmon Resonance Spectroscopy. *Anal. Chem.* **2014**, *86*, 5929–5936.